

Thermal bremsstrahlung probing the nuclear liquid-gas phase transition *

R. ORTEGA

Grup de Física de les Radiacions, Universitat Autònoma de Barcelona 08193 and
SUBATECH, 4, rue Alfred Kastler BP20722 44307 Nantes Cedex 3, France

AND

F. FERNÁNDEZ

Grup de Física de les Radiacions, Universitat Autònoma de Barcelona 08193,
D. D'ENTERRIA AND G. MARTÍNEZ

SUBATECH, 4, rue Alfred Kastler BP20722 44307 Nantes Cedex 3, France
FOR THE TAPS COLLABORATION

We present the results of the analysis of the hard photon production in the $^{129}\text{Xe} + \text{nat}\text{Sn}$ at 50A MeV system studied in the GANIL E300 experiment. The energy and angular hard photon distributions confirm the existence of a thermal component which follows the recently measured thermal bremsstrahlung systematics. Exploiting the performances of our complete detection system, consisting of TAPS and 3 charged particle multidetectors, we have also measured the hard photon multiplicity as a function of the charged particle multiplicity.

PACS numbers: 25.70.Pq, 21.65.+f

1. Introduction

One of the main issues in heavy-ion reactions at intermediate bombarding energies, from a few tens up to a hundred A MeV, is to determine the origin of nuclear multifragmentation. This process is characterized by an abundant production of intermediate-mass-fragments ($3 \leq Z \leq 20$) and it is the dominant decay channel observed in central nuclear collisions. The

* Presented at TAPS Workshop VI, Krzyże, Poland, September 9-13, 2001

interest of multifragmentation relies on its possible connection with the expected, though elusive, liquid-gas phase transition of nuclear matter [1, 2]. As a matter of fact, the origin and dynamics of multifragmentation are not yet clearly pinned down. On one extreme, sequential statistical approaches sustain that multifragmentation is the result of a slow and sequential fragment production process starting from a thermally equilibrated source [3]. On the other extreme, purely dynamical models assert that the fragmenting system has not reached global equilibrium when it disassembles in a prompt process [4, 5]. In between those extremes, fast statistical models [6, 7] rely on the attainment of (local) thermal equilibrium followed by a fast expansion of the hot nuclear systems which then break up according to the available phase space. All these seemingly different models reproduce well several patterns observed in the fragment production data. Therefore, to disentangle between them and shed some light on the connection between multifragmentation and the nuclear liquid-gas phase transition, one would need a new experimental observable contemporary to multifragmentation. We argue that thermal hard photons can be such a probe [11].

Hard photons are bremsstrahlung photons of energies above 30 MeV produced in proton-neutron collisions. Most part of the hard photon emission, the direct one, is produced in the initial preequilibrium stage of the reaction during the first compression of the system, but there is a softer second emission corresponding to the so-called thermal hard photons, which are emitted at intermediate stages of the reaction [8, 9]. Recently, the analysis of the data taken in Ar-induced reactions at 60A MeV by the TAPS collaboration at the Dutch-French AGOR cyclotron at KVI, has demonstrated that this second hard photon component really emerges from a thermalized source [11] during the time scale when the multifragmentation process is supposed to take place (50 fm/c-200 fm/c). Moreover, the measurement of a thermal hard photon emission in multifragmentation reactions in the $^{36}\text{Ar}+^{197}\text{Au}$ system has demonstrated that, at least for this reaction, the source breaks up after thermalization ($t \geq 80$ fm/c) [10, 11]. The observation of a thermally equilibrated radiating nuclear source opens up an interesting possibility in the study of the equation of state of nuclear matter in the region of the predicted liquid-gas phase transition [12].

The aim of the experiment E300 performed at GANIL in 1998 is to investigate the hard-photon production in multifragmentation reactions of the $^{129}\text{Xe}+^{\text{nat}}\text{Sn}$ at 50A MeV system [13]. The characteristics of this projectile-target combination (a large quasi-symmetric system with large energy deposition in the center-of-mass) makes of it a good candidate to study the liquid-gas transition. The existence/absence of a thermal hard-photon emission in multifragmentation reactions in such a system is expected to deliver, by means of a comparison with the previous KVI experimental results, a

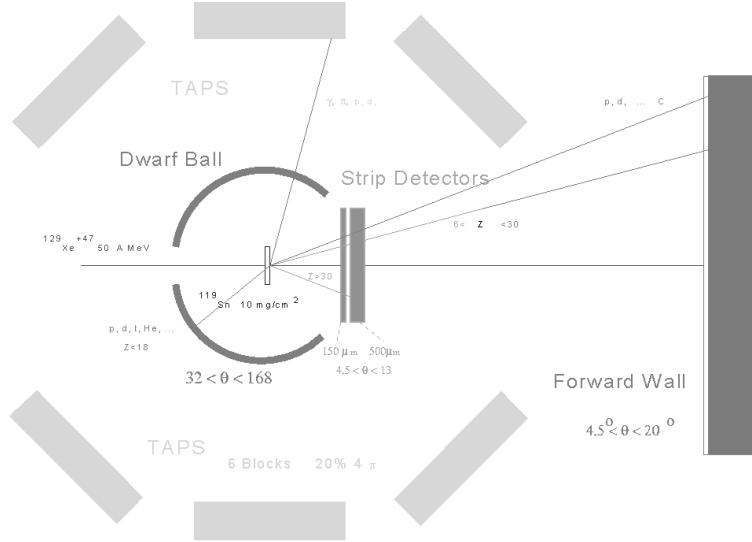


Fig.1. Schematic view of the experimental setup used to study the reaction $^{129}\text{Xe} + ^{\text{nat}}\text{Sn}$ at 50 A MeV. The detector system consisted of the “Silicon Strip Detector” (SSD), the “Dwarf Ball” (DB), the TAPS photon spectrometer and the “Forward Wall” (FW.)

more definite conclusion of the origin of nuclear multifragmentation.

2. Experimental set-up

To carry out this investigation inclusive and exclusive charged particle - photon measurements are necessary. For that purpose, the experimental setup of the E300 experiment (Fig. 1) consisted of the TAPS photon spectrometer coupled for the first time with three different charged-particle multidetectors: the “Silicon Strip Detector” (SSD), the Washington University “Dwarf Ball” (DB) and the KVI “Forward Wall” (FW). TAPS [14], arranged in 6 blocks of 64 BaF_2 each, allowed to measure photons of $5 \text{ MeV} < E_\gamma < 200 \text{ MeV}$ in 20 % of the full solid angle. The SSD [15], consisting of 64 circular and 128 radial silicon detectors, covered a forward angular range of $2.0^\circ \leq \theta \leq 10.3^\circ$. The SSD is sensitive to the intermediate-mass-fragments (IMF) and projectile-like-fragments (PLF) emitted at forward angles. The DB [16] is a multidetector consisting of 64 (BC400-CsITl) phoswich detectors forming a sphere surrounding the target and covering an angular range of $32^\circ \leq \theta \leq 168^\circ$. The DB permitted the identification of light-charged-particles (LCP) and IMF. The FW [17] is also a phoswich

multidetector, with 92 (NE115-NE102A) plastic modules, which allows the identification of LCP and IMF. The FW was placed downstream from the target covering the forward hemisphere ($2.5^\circ \leq \theta \leq 25^\circ$). The energy deposited by charged particles in the circular and radial strips of the SSD and in the individual crystal and plastic of each DB and FW phoswich were recorded. The charge of detected fragments and particles is identified by ΔE versus E analysis. The full details of the experimental setup and off-line analysis have been reported elsewhere [18, 19].

3. Experimental results

3.1. Inclusive hard photon results

After applying an energy correction factor to correct energy calibration and energy losses in the BaF₂ modules and subtracting the cosmic background we obtain the energy and angular spectra of the inclusive, i.e. without requiring any specific exit-channel condition, photon measurements [19].

In agreement with previous TAPS experiments we have found that the hard-photon energy spectrum measured in the NN center-of-mass (Fig. 2.a) is well reproduced with a double source fit, consisted of a sum of two exponential distributions:

$$\frac{dN}{dE_\gamma} = K_d e^{-E_\gamma/E_0^d} + K_t e^{-E_\gamma/E_0^t} \quad (3.1)$$

where the $K_{d,t}$ factors are defined by the direct and thermal hard-photon intensities, respectively. The harder hard-photon distribution with slope $E_0^d = 15.6 \pm 1.0$ MeV corresponds to the dominant direct component, whereas the softer one ($E_0^t = 7.0 \pm 0.6$ MeV) accounts for the thermal contribution, which amounts to 22% of the total intensity. Above $E_\gamma > 60$ MeV only the direct hard-photon emission is significant. The measured thermal slope, E_0^t , follows the recently observed linear dependence on the available energy in the nucleus-nucleus center-of-mass, E_{CC}^{AA} (Fig. 2.b) [11]. This observation is consistent with a thermal bremsstrahlung emission from secondary pn collisions. The obtained experimental thermal hard photon multiplicity $M_\gamma^{exp} = \sigma_\gamma^{exp} / \sigma_R^{exp} = (2.6 \pm 0.4)10^{-4}$.

We have analyzed the hard-photon angular distribution in two different energy ranges: the region of photons with $30 \text{ MeV} < E_\gamma < 40 \text{ MeV}$ and that of $E_\gamma > 60 \text{ MeV}$. The first energy region consists of a mixed distribution of direct and thermal photons and the latter exhibit their largest intensity, between 38% and 29% of the total hard photon yield. Whereas, as aforementioned, for $E_\gamma > 60 \text{ MeV}$ direct hard-photons clearly dominate. The measured (Doppler-shifted) laboratory angular distributions integrated

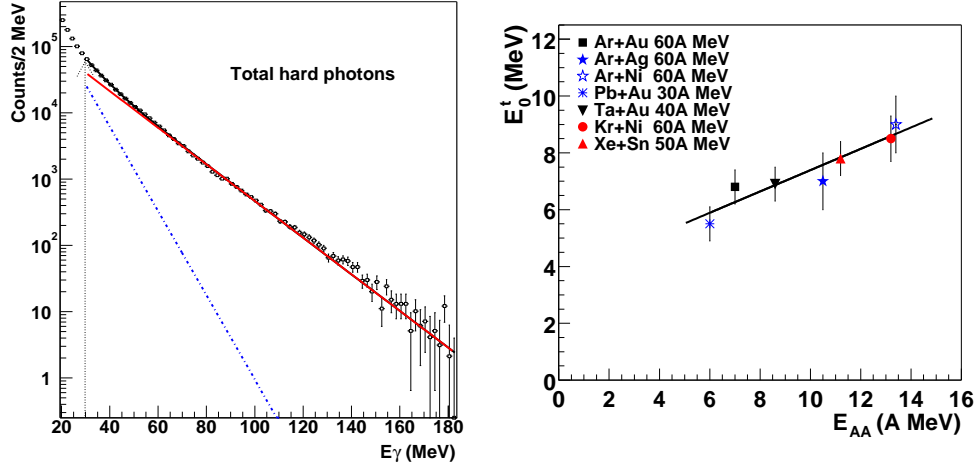


Fig. 2. a) The experimental inclusive hard photon spectrum measured for the reaction $^{129}\text{Xe} + ^{112}\text{Sn}$ in the NN center-of-mass frame fitted to Eq. (3.1). The thermal (dashed line) and direct (solid line) exponential contributions are shown. b) Thermal hard-photon slopes E_0^t , measured at $\theta_\gamma^{lab} = 90^\circ$, plotted as a function of the Coulomb-corrected nucleus-nucleus center-of-mass energy E_{CC}^{AA} . The measurements correspond to different TAPS experiments, the up triangle denotes the value of the reaction described in this contribution. The solid line is a linear fit to the data. Figure extracted from [11].

over the two energy ranges ($30 \text{ MeV} < E_\gamma < 40 \text{ MeV}$, and $E_\gamma > 60 \text{ MeV}$) have been respectively fitted according to the following expressions:

$$\left(\frac{dN}{d\Omega}\right)_{lab} = \frac{K}{Z^2} \left[1 - \alpha + \alpha \frac{\sin^2 \theta_\gamma^{lab}}{Z^2}\right] E_0 \left[e^{-30 \cdot Z/E_0} - e^{40 \cdot Z/E_0}\right] \quad (3.2)$$

$$\left(\frac{dN}{d\Omega}\right)_{lab} = \frac{K}{Z^2} \left[1 - \alpha + \alpha \frac{\sin^2 \theta_\gamma^{lab}}{Z^2}\right] E_0 e^{-60 \cdot Z/E_0} \quad (3.3)$$

where $Z = \gamma_S(1 - \beta_S \cos \theta_{lab})$, K is a normalization factor, β_S is the source velocity, α is the anisotropy factor and E_0 is the local slope. The velocity of the hard-photon source obtained in both fits is nearly the same, $\beta_S = 0.16 \pm 0.01$, and it agrees with the emission from a source moving with $\beta_S = \beta_{NN}$ but also, due to the symmetry of the $^{129}\text{Xe} + ^{nat}\text{Sn}$ system, with $\beta_S = \beta_{AA}$. Due to this symmetry, we have hence one free parameter less in the analysis of the angular distribution and therefore we are more sensitive to the fitting value of the anisotropy factor. The anisotropy

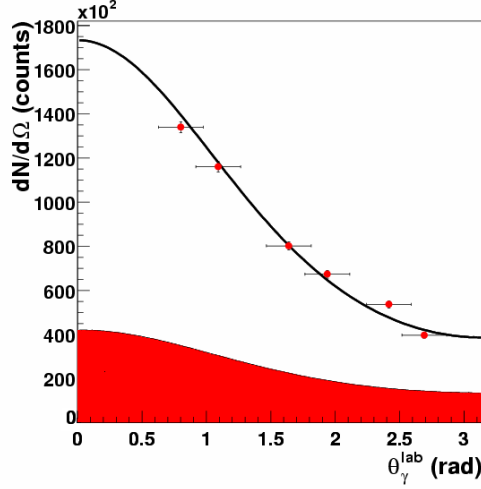


Fig. 3. Hard photon ($E_\gamma > 30$ MeV) angular distribution measured in the laboratory frame. The dark region is an estimation of the thermal hard-photon contribution.

factor is due to the existence of a preferential direction of the dipole component of the bremsstrahlung radiation in the elementary $pn \rightarrow pn\gamma$ process. This anisotropy should only appear in the radiation emerging from first-chance NN scattering, in which the momentum of the projectile nucleon still conserves its original (beam) direction. Indeed, we observe a non zero anisotropy factor, $\alpha = 0.2 \pm 0.1$, in the angular distribution measured for photons of $E_\gamma > 60$ MeV, which is dominated by the direct hard-photon component. In contrast, no anisotropy is found in the angular distribution of the mixed thermal and direct energy range ($30 \text{ MeV} < E_\gamma < 40 \text{ MeV}$): $\alpha = 0.0 \pm 0.1$. Thus, these slightly different (within their associated fitting errors) α values can be interpreted as an indication of the distinct origins of the two hard-photon contributions. Finally, the total ($E_\gamma > 30$ MeV) hard photon angular emission (Fig. 3) can be well reproduced with the expression:

$$\left(\frac{dN}{d\Omega}\right)_{lab} = \frac{K^d}{Z^2} \left[1 - \alpha + \alpha \frac{\sin^2 \theta_\gamma^{lab}}{Z^2} \right] E_0^d e^{-30 Z/E_0^d} + \frac{K^t}{Z^2} E_0^t e^{-30 Z/E_0^t} \quad (3.4)$$

The values of the direct/thermal and the ratio of intensities are those measured in the energy spectrum.

3.2. Exclusive hard photon measurements

In our previous analysis we have focused on the global properties of the hard photon emission. However, if we want to shed light on the mechanism leading to multifragmentation and to extract the thermodynamical properties of a possibly thermalized photon source, we have to select the more interesting (though less probable) central and semi-central reactions, and analyze the hard photon production emitted in such collisions. LCP and IMF multiplicities will allow us to define the impact-parameter selection criteria. Next, we present our first exclusive photon measurements: the correlation of photon multiplicities for 3 energy ranges with the charged particle multiplicities measured in the DB and FW detectors. We will consider three energy regions: $10 \text{ MeV} < E_\gamma < 22 \text{ MeV}$ and hard-photons of $30 \text{ MeV} < E_\gamma < 40 \text{ MeV}$ and $E_\gamma > 60 \text{ MeV}$. The two regions of hard-photons have been chosen due to the reasons explained in the analysis of the angular distribution. Photons of energies between 10-20 MeV come mainly from the decay of Giant-Dipole Resonances (GDR) produced in the moderated excited fragments and, unlike hard photons, are produced by a collective mechanism. As Fig. 4.a shows, one can separate the two hard photon components from GDR photons by the dependence of their multiplicities on the DB charged particle multiplicity. Whereas both hard photon components increase with the charged particle multiplicity, i.e with the centrality, GDR photons exhibit a maximum at peripheral reactions. Fig. 4.b shows the same histogram of M_γ versus M_{CP}^{DB} with the additional condition on the charged particle multiplicity measured in the FW: $M_{CP}^{FW}=2-4$, where the photon multiplicity exhibits a maximum. In this case, we observed the maximum enhancement of hard-photons with charged particle multiplicity: a factor 10 between $M_{CP}^{DB}=1$ and $M_{CP}^{DB}=11$.

4. Summary and Outlook

In summary, we have analysed the inclusive hard photon spectrum of the $^{129}\text{Xe} + \text{nat}\text{Sn}$ at 50A MeV reaction. The double-source analysis (a double exponential fit with two different inverse slope parameters) shows that the hard-photon distribution is consistent with a direct plus a thermal proton-neutron bremsstrahlung contributions, accounting for 78 % and 22 % of the total hard-photon yield, respectively. The measured thermal slope, E_0^t , follows the recently observed linear dependence on the available energy in the nucleus-nucleus center-of-mass E_{Cc}^{AA} , confirming a thermal nature of the secondary bremsstrahlung emission. In the analysis of the hard-photon angular emission we have observed an isotropic emission of hard photons in the $30 \text{ MeV} < E_\gamma < 40$ range, consistent with the existence of a thermal component coming from second-chance NN collisions which blurs the

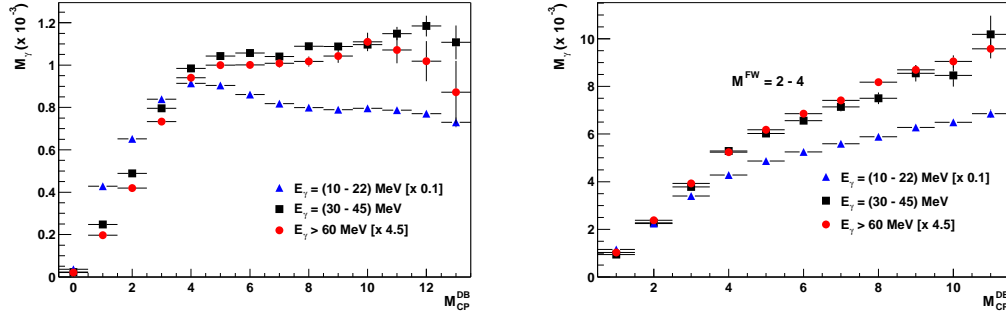


Fig. 4. a) Photon multiplicity, M_γ , as a function of the charged particle multiplicity measured in the DB, M_{CP}^{DB} . b) The same measurement with the condition of a charged particle multiplicity measured in the FW, M_{CP}^{FW} , between 2 and 4, the region of M_{CP}^{FW} in which the photon multiplicity exhibits a maximum.

original elementary anisotropy present in the prompt direct hard photon emission. In the exclusive hard photon measurements, we have studied the dependence of the photon multiplicities on the impact parameter. We are presently, carrying out the same type of analysis of the energy and angular hard-photon spectra in reactions in which multifragmentation is the most probable exit-channel, as well as in peripheral collisions, so that we can extract a definite conclusion about thermal hard-photon production in multifragment reactions.

REFERENCES

- [1] L.G. Moretto, Annu. Rev. Nucl. Part. Sci. **379**, (1993).
- [2] S. Das Gupta *et al.*, nucl-th/0009033.
- [3] W. Friedman, Phys. Rev. C **42**, 667 (1990).
- [4] M. Baldo *et al.*, Phys. Rev **C51**, 1 (1995).
- [5] J. Aichelin, Phys. Rep. **202**, 233 (1991).
- [6] A.S. Botvina, Nucl. Phys. **A475**, 663 (1987).
- [7] D.H.E. Gross, Nucl. Phys. **A553**, 175 (1993).
- [8] G. Martínez *et al.*, Phys. Lett. **B349**, 23 (1995).
- [9] Y. Schutz *et al.*, Nucl. Phys. **A622**, 404 (1997).
- [10] D. d'Enterria, Ph.D.Thesis, Univ. de Caen and Univ. Aut. de Barcelona, 2000.
- [11] D. d'Enterria *et al.*, Phys. Rev. Lett. **87**, 22701 (2001).
- [12] D. d'Enterria *et al.*, in preparation.

- [13] G. Martínez Acta Phys. Pol. **29**, 232 (1997).
- [14] R. Novotny, IEEE Trans. Nucl. Sci. **38**, 379 (1991).
- [15] M. Josset, Ph.D. Thesis, Université de Caen, 1996.
- [16] D. Stracener *et al.*, Nucl. Ins. and Meth. **A294**, 485 (1990).
- [17] S. Luke *et al.*, Phys. Rev. **47**, 1211 (1993).
- [18] R. Ortega, Proceedings of TAPS V Workshop, Czech Journal of Physics (2000).
- [19] R. Ortega, Treball de recerca, Univ. Autònoma de Barcelona (2001).